NRC-CNRC

From Discovery
to Innovation...
De la découverte
à l'innovation...

La Science à l'œuvre pour le
at work for Canada

NRC Publications Archive
Archives des publications du CNRC

Numerical solutions of three-dimensional non-grey gas radiative transfer using the statistical narrow-band model
Liu, Fengshan

This publication could be one of several versions: author's original, accepted manuscript or the publisher's version. /
La version de cette publication peut être l'une des suivantes : la version prépublication de l'auteur, la version acceptée du manuscrit ou la version de l'éditeur.

For the publisher's version, please access the DOI link below./ Pour consulter la version de l'éditeur, utilisez le lien DOI ci-dessous.

NRC Publications Record / Notice d'Archives des publications de CNRC:
http://nparc.cisti-icist.nrc-cnrc.gc.ca/npsi/ctrl?action=rtdoc&an=12326942&lang=en
http://nparc.cisti-icist.nrc-cnrc.gc.ca/npsi/ctrl?action=rtdoc&an=12326942&lang=fr

National Research
Council Canada

Conseil national
de recherches Canada

Canada

Chen, J. C., 1966, "Laminar Heat Transfer in a Tube with Nonlinear Radial Heat-Flux Boundary Conditions," *Int. J. Heat Mass Transfer*, Vol. 9, pp. 433–440.

Cheng, C. H., Weng, C. J., and Aung, W., 1995, "Buoyancy Effect on the Flow Reversal of Three-Dimensional Developing Flow in a Vertical Rectangular Duct—A Parabolic Model Solution," ASME JOURNAL OF HEAT TRANSFER, Vol. 117, pp. 238–241.

Cheng, K. C., and Yuen, F. P., 1985, "Flow Visualization Studies on Secondary Flow Pattern for Mixed Convection in the Entrance Region of Isothermally Heated Inclined Pipes," *Fundamentals of Forced and Mixed Convection*, ASME HTD-Vol. 42, pp. 121–130.

Chou, F. C., and Hwang, G. J., 1987, "Vorticity-Velocity Method for Graetz Problem with the Effect of Natural Convection in a Horizontal Rectangular Channel with Uniform Wall Heat Flux," ASME JOURNAL OF HEAT TRANSFER, Vol. 109, pp. 704–710.

Choudhury, D., and Patankar, S. V., 1988, "Combined Forced and Free Laminar Convection in the Entrance Region of an Inclined Isothermal Tube," ASME JOURNAL OF HEAT TRANSFER, Vol. 110, pp. 901–909.

Fiveland, W. A., 1988, "Three-Dimensional Radiative Heat Transfer Solutions by the Discrete-Ordinates Method," *AIAA J. Thermophysics and Heat Transfer*, Vol. 2, pp. 309–316.

Hishida, M., Nagano, Y., and Montesclaros, M. S., 1982, "Combined Forced and Free Convection in the Entrance Region of an Isothermally Heated Horizontal Pipe," ASME JOURNAL OF HEAT TRANSFER, Vol. 104, pp. 153–159.

Huang, J. M., Lin, J. D., and Chou, F. C., 1990, "Combined Radiation and Laminar Mixed Convection in the Thermal Entrance Region of Horizontal Isothermal Rectangular Channels," *Numer. Heat Transfer*, Part A, Vol. 18, pp. 113–125.

Incropera, F. P., Knox, A. L., and Maughan, J. R., 1988, "Effect of Wall Heat Flux Distribution on Laminar Mixed Convection in the Entry Region of a Horizontal Rectangular Duct," *Numer. Heat Transfer*, Vol. 13, pp. 427–450.

Kim, T. A., and Baek, S. W., 1991, "Analysis of Combined Conductive and Radiative Heat Transfer in a Two-Dimensional Rectangular Enclosure Using the Discrete Ordinates Method," *Int. J. Heat Mass Transfer*, Vol. 34, pp. 2265–2273.

Mahaney, H. V., Incropera, F. P., and Ramadhyani, S., 1987, "Development of Laminar Mixed Convection Flow in a Horizontal Rectangular Duct with Uniform Bottom Heating," *Numer. Heat Transfer*, Vol. 12, pp. 137–155.

Modest, M. F., 1993, *Radiative Heat Transfer*, McGraw-Hill, New York, pp. 541–571.

Morcos, E. M., and Abou-Ellail, M. M. M., 1983, "Buoyancy Effects in the Entrance Region of an Inclined Multirectangular Channel Solar Collector," ASME *Journal of Solar Energy Engineering*, Vol. 105, pp. 157–162.

Morcos, S. M., Hilal, M. M., Kamel, M. M., and Soliman, M. S., 1986, "Experimental Investigation of Mixed Laminar Convection in the Entrance Region of Inclined Rectangular Channels," ASME JOURNAL OF HEAT TRANSFER, Vol. 108, pp. 574–579.

Roache, P. J., 1971, *Computational Fluid Dynamics*, Reinhold, New York, pp. 61–64.

Wassel, A. T., and Edwards, D. K., 1976, "Molecular Radiation in a Laminar or Turbulent Pipe Flow," ASME JOURNAL OF HEAT TRANSFER, Vol. 98, pp. 101–107.

Yan, W. M., 1994, "Mixed Convection Heat and Mass Transfer in Inclined Rectangular Ducts," *Int. J. Heat Mass Transfer*, Vol. 37, pp. 1857–1866.

Yan, W. M., 1995, "Transport Phenomena of Developing Laminar Mixed Convection Heat and Mass Transfer in Inclined Rectangular Ducts," *Int. J. Heat Mass Transfer*, Vol. 38, pp. 2905–2914.

Numerical Solutions of Three-Dimensional Non-Grey Gas Radiative Transfer Using the Statistical Narrow-Band Model

F. Liu[1]

Three-dimensional non-grey gas radiation analyses were conducted using the statistical narrow-band model along with up-dated band parameters. The exact narrow-band averaged radiative transfer equation was solved using a ray-tracing method. Accurate numerical results were presented for non-grey real gas radiative transfer in a three-dimensional rectangular enclosure containing (i) an isothermal pure water vapor at 1000 K and 1 atm, (ii) an isothermal and inhomogeneous H_2O/N_2 mixture at 1000 K and 1 atm, and (iii) a nonisothermal and homogeneous mixture of $CO_2/H_2O/N_2$ at 1 atm.

[1] Associate Research Officer, Combustion Technology, Institute for Chemical Process and Environmental Technology, National Research Council, Ottawa, ON K1A 0R6, Canada. e-mail: fengshan.liu@ncr.ca.

1 Introduction

Development of computationally efficient and accurate gas radiative property models for non-grey gas radiation analysis has been an active research subject in recent years. Most of the research attention has been paid to develop absorption coefficient-based models due to its compatibility with the radiative transfer equation (RTE) in standard form. These include the weighted-sum-of-grey-gases models (Hottel and Sarofim, 1967; Denison and Webb, 1993) and the K-distribution method (Goody and Yung, 1989) as well as its variants (Lee et al., 1996; Parthasarathy et al., 1996).

Band models appear to be attractive in terms of efficiency and accuracy based on their principles. However, their applications to multidimensional problems are seriously restricted by the following two factors. First, band models provide band transmissivity rather than the fundamental property, i.e., gas absorption coefficient. As a consequence, most of the solution methods cannot be readily used. Secondly, band averaging of the RTE gives rise to additional source terms which are very difficult to deal with and require much more computing time (Kim et al., 1991; Liu et al., 1997). Despite the difficulties of applying band models to multidimensional problems, results of narrow-band models are often treated as accurate and used as benchmark solution in the evaluation of other approximate models when exact line-by-line (LBL) results are not available (Soufiani and Djavdan, 1994; Parthasarathy et al., 1996; Bedir et al., 1997).

Non-grey gas radiation results reported in the literature are either for *real gases*, i.e., H_2O and CO_2, in one-dimensional parallel-plates geometry; e.g., Kim et al. (1991), Denison and Webb (1993), or for "synthetic gas" with specified gas absorption coefficient in three dimensions, such as those based on Edwards' exponential wide-band model and the Elsasser model for line structure (Tang and Brewster, 1994). Accurate results of three-dimensional non-grey radiation analysis of real gases are typically lacking, primarily due to the unacceptable computing time required by performing LBL calculations in multidimensions. With this situation in mind, the present work aims at reporting accurate numerical results of three-dimensional non-grey gas radiation using the statistical narrow-band (SNB) model in inhomogeneous and nonisothermal media. These results are useful in evaluating the accuracy of other approximate gas radiation models.

2 Numerical Method and the Statistical Narrow-Band Model

The exact narrow-band averaged RTE presented by Kim et al. (1991) was solved using a ray-tracing method in three-dimensional Cartesian coordinates. Interested readers should refer to the papers by Kim et al. (1991) and Liu et al. (1997) for details. The ray-tracing method used in this work is essentially a modified version of the discrete transfer method developed by Lockwood and Shah (1981) to improve its accuracy in the calculation of the radiative source term. The method is briefly outlined below. For a given control volume, ray-tracing is performed at the center of each control surface (six in three dimensions) along all the directions defined by a T_N quadrature set (Thurgood et al., 1995) to obtain radiation intensities. The net radiative fluxes at these control surface centers were evaluated

Table 1 Conditions of the three test cases

Case	Temperature distribution	Gas mixture compositions
1	uniform, 1000 K	uniform, pure water vapour
2	uniform, 1000 K	non-uniform H_2O/N_2 mixture
3	non-uniform	uniform, $CO_2/H_2O/N_2$ mixture

Table 2 Distributions of radiative source term along the centerline and wall heat flux density along (2 m, 1 m, z) for the first case

z, m	Radiative source, kW m^{-3}	Heat flux density, kW m^{-2}
0.125	−91.962	25.679
0.375	−32.189	28.992
0.625	−25.708	30.047
0.875	−22.708	30.620
1.125	−21.654	30.966
1.375	−21.220	31.103
1.625	−21.043	31.202
1.875	−20.742	31.273

Table 3 Distributions of radiative source along (x, 1 m, 0.375 m) and wall heat flux density along (x, 1 m, 4 m) for the first case

x, m	Radiative source, kW m^{-3}	Heat flux density, kW m^{-2}
0.0909	−115.560	24.953
0.2727	−46.429	28.487
0.4546	−36.741	29.732
0.6364	−34.114	30.324
0.8182	−32.699	30.692
1.0000	−32.189	30.915
1.1819	−32.699	30.692
1.3637	−34.114	30.324
1.5455	−36.741	29.732
1.7274	−46.429	28.487
1.9092	−115.560	24.953

from the known radiation intensity and the weight function of the T_N set, a common practice of the discrete-ordinates method. The same procedure is repeated for all the narrow bands. The radiative source term at the control volume under consideration is then found by taking the divergence of the total net heat flux using a straightforward finite difference. This procedure is very time-consuming and is not recommended for other applications. It was developed in this work only for the purpose of obtaining accurate results of the narrow-band averaged RTE in three dimensions.

The SNB model (Ludwig et al., 1973) was used in the present calculations to provide narrow-band gas transmissivity of CO_2 and H_2O. The updated band parameters described by Soufiani and Taine (1997) were employed. For calculations in inhomogeneous and/or nonisothermal media, the Curtis-Godson approximation was used.

3 Description of Test Problems

The geometry of the test problems is a rectangular enclosure of 2 m × 2 m × 4 m. All the surrounding walls are black and cold at 300 K. The pressure of the gas mixture in the enclosure is kept at 1 atm for all the cases. Three cases are considered and are summarized in Table 1.

In the second test case, the medium is a nonuniform mixture of H_2O and N_2 with the mole fraction of H_2O specified by $x_{H_2O} = 4(z/L_z)(1 - z/L_z)$, where $L_z = 4$ m. In the third test case, the medium is assumed to be a mixture of $0.1CO_2 + 0.2H_2O + 0.7N_2$ (mole basis). The gas temperature is nonuniform but symmetrical about the centerline of the enclosure and is specified in terms of $T = (T_c - T_e)f(r/R) + T_e$. In this equation, T_c is the gas temperature along the centerline of the enclosure, T_e is the exit temperature at $z = 4$ m. Inside the circular region of the cross section of the enclosure, the variation of gas temperature is defined by $f(r/R) = 1 - 3(r/R)^2 + 2(r/R)^3$, where r is the distance from the enclosure centerline and R is the radius of the circular region ($R = 1$ m). The gas temperature outside the circular region is assumed to be uniform and at the value of the exit temperature. The centerline temperature is assumed to increase linearly from 400 K at the inlet ($z = 0$) to 1800 K at $z = 0.375$ m, then decreases linearly to 800 K at the exit.

4 Results and Discussion

Due to enormous computing time required to carry out the present calculations, numerical results tabulated in this section are obtained using relatively coarse grids and the T_4 quadrature set (128 directions). However, the grid independence of these results were checked by calculating the source term distribution along the centerline of the enclosure using finer grids, since the calculation of source term is more sensitive to grid division than that of heat flux. The effect of angular discretisation on the results was examined in the third case by performing the calculations using the T_4 and the T_6 (288 directions) sets. It was found that the results calculated using the T_4 set differ from those obtained using the T_6 set by only one percent.
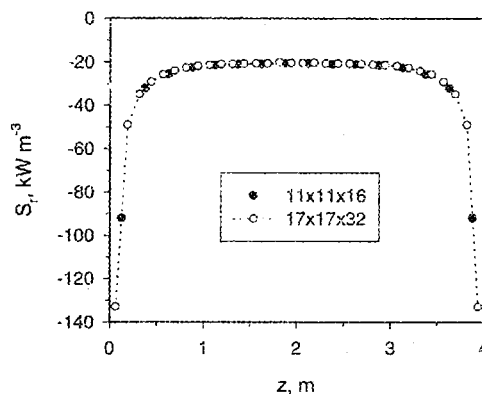
The first case was calculated using a 11 × 11 × 16 uniform grid. The calculated radiative source terms along the centerline of the enclosure, (1 m, 1 m, z), and the wall heat flux densities

Fig. 1 Comparison of source term distributions along the centerline of the enclosure calculated using two computational grids for the first test case

along (2 m, 1 m, z) are tabulated in Table 2 for half of the enclosure due to the symmetry of this problem. Table 3 displays the radiative source terms along (x, 1 m, 0.375 m) and wall heat flux densities along (x, 1 m, 4 m).

An additional run was carried out in this case using a finer uniform grid, 17 × 17 × 32, for source terms along the centerline only in order to confirm that the results shown in Tables 2 and 3 are grid independent. Results obtained using the coarse and the fine grids are compared in Fig. 1. It can be seen that they are almost identical. In addition, the source term distributions shown in Fig. 1 and Table 3 are qualitatively similar to those obtained in one-dimensional parallel-plates enclosure (Kim et al., 1991; Liu et al., 1997).
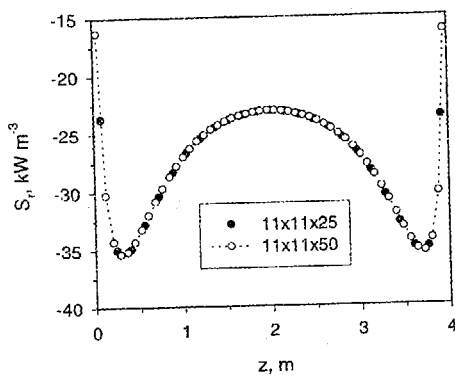
The second case was calculated using a 11 × 11 × 25 uniform grid. Results of the second case are summarized in Tables 4 and 5.

Table 4 Distributions of radiative source term along the centerline and wall heat flux density along (2 m, 1 m, z) for the second case

z, m	Radiative source, kW m^{-3}	Heat flux density, kW m^{-2}
0.08	−23.681	11.942
0.24	−35.010	15.825
0.40	−34.934	19.090
0.56	−32.830	21.617
0.72	−30.425	23.560
0.88	−28.327	25.064
1.04	−26.663	26.236
1.20	−25.416	27.148
1.36	−24.503	27.841
1.52	−23.858	28.351
1.68	−23.443	28.701
1.84	−23.189	28.906
2.00	−23.090	28.973

Table 5 Distributions of radiative source along (x, 1 m, 0.24 m) and wall heat flux density along (x, 1 m, 4 m) for the second case

x, m	Radiative source, kW m^{-3}	Heat flux density, kW m^{-2}
0.0909	−60.316	15.529
0.2727	−41.372	19.275
0.4546	−37.405	20.916
0.6364	−35.918	21.799
0.8182	−35.208	22.380
1.0000	−35.010	22.719
1.1819	−35.208	22.380
1.3637	−35.918	21.799
1.5455	−37.405	20.916
1.7274	−41.372	19.275
1.9092	−60.316	15.529

Table 6 Distributions of radiative source along the centerline and heat flux density along (2 m, 1 m, z) for the third case

z, m	Radiative source, kW m^{-3}	Heat flux, kW m^{-2}
0.040	69.146	11.288
0.115	59.081	13.120
0.190	−11.900	14.644
0.265	−156.04	16.170
0.325	−318.16	16.949
0.375	−531.15	17.529
0.425	−439.46	18.300
0.500	−390.36	19.286
0.600	−354.02	19.901
0.725	−321.33	20.236
0.875	−291.59	20.518
1.025	−267.15	20.614
1.200	−240.06	20.210
1.400	−210.62	19.485
1.600	−184.39	18.620
1.800	−161.07	17.722
2.000	−139.90	16.835
2.250	−112.68	15.762
2.550	−85.092	14.488
2.850	−61.041	13.252
3.125	−43.583	12.136
3.375	−31.102	11.137
3.625	−20.995	10.101
3.875	−25.320	8.483

Fig. 3 Comparison of source term distributions along the centerline of the enclosure calculated using two computational grids for the third test case
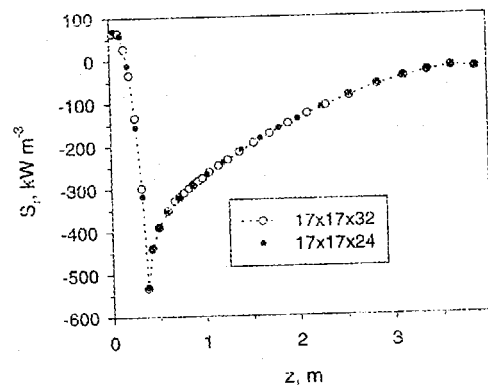

Fig. 2 Comparison of source term distributions along the centerline of the enclosure calculated using two computational grids for the second test case

In order to check the adequacy of the grid division for the results given in Tables 4 and 5, the source terms along the centerline of the enclosure were also calculated using a uniform grid of 11 × 11 × 50. Results obtained using the two grids are compared in Fig. 2. Again, the two grids yield almost identical results. Fig. 2 confirms that the use of the relatively coarse grid of 11 × 11 × 25 is adequate for this case. The W-shaped source term distribution shown in Fig. 2 is similar to that obtained in one-dimensional parallel-plates enclosure (Kim et al., 1991). The left valley of the W-shape occurs at about z = 0.28 m.

Calculations of the third case were conducted using a nonuniform grid. The computational grid used was 17 × 17 × 24. Uniform grid division was used in the x and y directions and

the grid division in the z direction was nonuniform with finer grids placed around the peak gas temperature (z = 0.375 m). Representative results of this case are tabulated in Table 6.

Grid independence of the results given in Table 6 is demonstrated in Fig. 3 by comparing the results of source term along the centerline calculated using two grids. Once again, the effect of grid size on the results is seen to be negligible. The shape of the source term distribution is expected from the specifications of species and temperature fields. It is interesting to observe that the source term reaches its minimum at the same location as the gas temperature, indicating the dominant influence of local gas emission. However, the wall heat flux density shown in Table 6 peaks further downstream at around z = 1.025 m, reflecting the long-distance nature of thermal radiation.

5 Conclusions

Three-dimensional non-grey gas radiation analyses were conducted using the statistical narrow-band model with updated band parameters. The exact narrow-band averaged radiative transfer equation was solved using a ray-tracing technique along with the T_N quadrature set. Accurate numerical results were reported for

non-grey gas radiation in a rectangular enclosure containing three different gas mixtures. These results are valuable for future evaluation of other non-grey gas radiation models.

Acknowledgments

References

Bedir, H., T'ien, J. S., and Lee, H. S., 1997, "Comparison of Different Radiation Treatments for a One-Dimensional Diffusion Flame," *Combust. Theory Modelling*, Vol. 1, pp. 395–404.

Denison, M. K., and Webb, B. W., 1993, "A Spectral Line-Based Weighted-Sum-of-Gray-Gases Model for Arbitrary RTE Solvers," ASME JOURNAL OF HEAT TRANSFER, Vol. 115, pp. 1004–1011.

Goody, R. M., and Yung, Y. L., 1989, *Atmospheric Radiation*, 2nd Ed. Oxford University Press, Oxford, UK.

Hartmann, J. M., Levi Di Leon, R., and Taine, J., 1984, "Line-by-Line and Narrow-Band Statistical Model Calculation for H₂O," *Journal of Quantitative Spectroscopy and Radiative Transfer*, Vol. 32, No. 2, pp. 119–127.

Hottel, H. C., and Sarofim, A. F., 1967, *Radiative Transfer*, McGraw-Hill, New York.

Kim, T.-K., Menart, J. A., and Lee, H. S., 1991, "Nongray Radiative Gas Analysis Using the S-N Discrete Ordinates Method," ASME JOURNAL OF HEAT TRANSFER, Vol. 113, pp. 946–952.

Lee, P. Y. C., Hollands, K. G. T., and Raithby, G. D., 1996, "Reordering the Absorption Coefficient within the Wide Band for Predicting Gaseous Radiant Exchange," ASME JOURNAL OF HEAT TRANSFER, Vol. 118, pp. 394–400.

Liu, F., Gülder, Ö. L., Smallwood, G. J., and Ju, Y., 1997, "Non-Grey Gas Radiative Transfer Analyses Using the Statistical Narrow-Band Model," *Int. J. Heat Mass Transfer*, to appear.

Lockwood, F. C., and Shah, N. G., 1981, "A New Radiation Solution Method for Incorporation in General Combustion Prediction Procedures," *18th Symposium (International) on Combustion*, The Combustion Institute, pp. 1405–1413.

Ludwig, D. B., Malkmus, W., Reardon, J. E., and Thomson, J. A. L., 1973, "Handbook of Infrared Radiation from Combustion Gases," NASA SP3080.

Parthasarathy, G., Chai, J. C., and Patankar, S. V., 1996, "A Simple Approach to Non-Gray Gas Modeling," *Numerical Heat Transfer*, Part B, Vol. 29, pp. 113–123.

Soufiani, A., and Djavdan, E., 1994, "A Comparison between Weighted Sum of Gray Gases and Statistical Narrow-Band Radiation Models for Combustion Applications," *Combustion and Flame*, Vol. 97, pp. 240–250.

Soufiani, A., and Taine, J., 1997, "High Temperature Gas Radiative Property Parameters of Statistical Narrow-Band Model for H₂O, CO₂ and CO and Correlated-K (CK) Model for H₂O and CO₂," *Int. J. Heat Mass Transfer*, Vol. 40, pp. 987–991.

Tang, K. C., and Brewster, M. Q., 1994, "K-Distribution Analysis of Gas Radiation with Nongray, Emitting, Absorbing, and Anisotropic Scattering Particles," ASME JOURNAL OF HEAT TRANSFER, Vol. 116, pp. 980–985.

Thurgood, C. P., Pollard, A., and Becker, A. B., 1995, "The T_N Quadrature Set for the Discrete Ordinates Method," ASME JOURNAL OF HEAT TRANSFER, Vol. 117, pp. 1068–1070.

Application of Adaptive Quadrature to Fire Radiation Modeling

P. S. Cumber[1]

Nomenclature

E_{bound} = error bound
E_{est} = error estimate
G_1, P_2, P_i = labels for ray orientations
I = spectrally integrated intensity

[1] BG Technology, Gas Research & Technology Centre, Loughborough LE11 3GR, UK. e-mail: peter.cumber@bgtech.co.uk.

I_λ = spectral intensity
N_{bad} = radius of refinement
N_θ, N_φ = number of rays in the θ and φ coordinate directions
q_- = incident flux
s = point vector

Introduction

The accurate modeling of thermal radiation is important in many combusting systems. The radiative flux incident to a point s on a surface or a radiometer can be expressed by the integral

$$q_- = \int_{\Delta\Omega} \int_0^\infty I_\lambda(\Omega, s) \cos \theta d\lambda d\Omega \qquad (1)$$

where I_λ is the spectral intensity, λ denotes wavelength, θ is the angle of incidence, and $\Delta\Omega$ is the field of view of the receiver. Taking scattering to be negligible, the spectral intensity distribution can be calculated, for example, by an exponential wideband model (e.g., Cumber et al., 1998); alternatively, the spectral integration is avoided and the total intensity is calculated using a more empirical approach, such as a mixed-grey-gas model (e.g., Truelove, 1976).

In this note an adaptive quadrature strategy over a solid-angle implemented as part of the discrete transfer method (Lockwood and Shah, 1981) is presented and evaluated by calculating the received radiation about two natural gas jet fires. The calculation of the external radiation field of a jet fire is a particularly challenging task, as the intensity field is highly anisotropic with a small hot volume of gas dominating the heat transfer external to the flame envelope.

Flame Structure Model

The first jet fire considered is a laboratory scale rim-stabilized axisymmetric methane flame. The flame has a Reynolds number of 8800 based on the bulk velocity at the nozzle exit. The nozzle has a diameter of 8.4 mm. More details of the experiment can be found in Cumber et al. (1998). This flow is computationally inexpensive to calculate, and turbulence-radiation interaction effects have been found to be small (Jeng et al., 1984), making it possible to use a mean flow-field analysis to model the external radiation field. The modeling of the radiation flux requires some representation of the flame structure, which is predicted using a model based on the boundary layer equations, (Spalding, 1977). A detailed description of the model can be found in Cumber et al. (1998).

The sonic natural gas jet fire considered below has a pressure ratio of 1.68 issuing from a stack with a diameter of 385 mm into an atmospheric boundary layer with a wind speed of 6.2 m/s measured at a height of 10 m. The full details of the field scale test and the reacting flow simulation can be found in Cook et al. (1997).

Radiation Modeling

In the discrete transfer method, to evaluate the incident flux integral it is expressed in spherical coordinates and the field of view discretized with a uniform spacing in the angle of rotation (φ) and angle of incidence (θ). For the remainder of this article such a distribution of rays will be described as "uniform." The incident intensity distribution is assumed piecewise constant over the field of view of the receiver. The incident intensity over an element is calculated by tracing the ray with orientation defined by its centroid, through the computational domain, noting the control volumes of the finite volume grid traversed, length of ray segment, and local thermochemical quantities. The ray trace is terminated at the computational boundary. The stored data is then used as an input to a model for participating